

NASA Technical Memorandum 102494

# Experimental Investigations on Channelized Coplanar Waveguide

Rainee N. Simons  
*Case Western Reserve University*  
*Cleveland, Ohio*

George E. Ponchak  
*Lewis Research Center*  
*Cleveland, Ohio*

Konstantinas S. Martzaklis  
*University of Akron*  
*Akron, Ohio*

and

Robert R. Romanofsky  
*Lewis Research Center*  
*Cleveland, Ohio*

April 1990

**NASA**



# EXPERIMENTAL INVESTIGATIONS ON CHANNELIZED COPLANAR WAVEGUIDE

Rainee N. Simons\*  
Case Western Reserve University  
Cleveland, Ohio 44106

George E. Ponchak  
National Aeronautics and Space Administration  
Lewis Research Center  
Cleveland, Ohio 44135

Konstantinos S. Martzaklis†  
University of Akron  
Akron, Ohio

Robert R. Romanofsky  
National Aeronautics and Space Administration  
Lewis Research Center  
Cleveland, Ohio 44135

## SUMMARY

This paper presents a new variant of coplanar waveguide (CPW) which has been termed channelized coplanar waveguide (CCPW). Measured propagation characteristics for CCPW such as  $\epsilon(\text{eff})$  and unloaded  $Q$  as a function of geometrical parameters and frequency are presented. The measured and modeled  $\epsilon(\text{eff})$  are also compared. Equivalent circuit model element values are presented for a CCPW open circuit and a CCPW right angle bend. A CCPW matched T-junction, matched 1:3 junction, and a novel coax-to-CCPW in-phase, N-way, radial power divider are also demonstrated.

## INTRODUCTION

Coplanar waveguide, CPW, on a dielectric substrate consists of a center strip conductor with semi-infinite ground planes on either side (ref. 1). A variant of CPW is grounded coplanar waveguide, GCPW, which has an additional ground plane on the opposite side of the substrate to facilitate heat removal and packaging (ref. 2). These transmission lines have several advantages which make them ideally suited for microwave integrated circuits. The disadvantage of CPW and GCPW is that the structure can support spurious modes besides the CPW mode since the transverse dimensions may be several wavelengths.

This paper presents a new variant of CPW. The new structure has side walls which, together with the ground plane, constitute a channel and hence is

---

\*NASA Resident Research Associate at Lewis Research Center (work funded by NASA Grant NAG3-816).

†Student Co-op at NASA Lewis Research Center.

appropriately termed as channelized coplanar waveguide, CCPW. A shielding structure may also be used to further confine the electromagnetic fields. This structure is shown in figure 1. The enclosure of the CPW transmission line eliminates radiation loss and spurious surface modes created at discontinuities. Also, because the basic transmission line structure is CPW, CCPW maintains the inherent advantages over microstrip for easy shunt as well as series mounting of active and passive components.

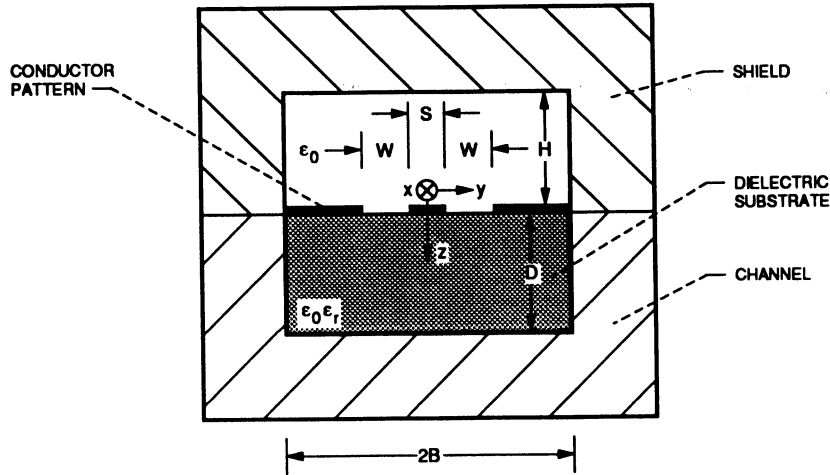


Figure 1. - Schematic of channelized coplanar waveguide (CCPW).

To maintain a single CPW mode of propagation, CCPW must be designed to suppress the dielectric filled rectangular waveguide mode, the microstrip mode, and the rectangular coax mode. The channel width,  $2B$ , is chosen such that the rectangular waveguide mode is cutoff. The microstrip and rectangular coax modes are suppressed by the proper selection of the slot width,  $W$ , the center strip width,  $S$ , and the substrate thickness,  $D$ . The ratios  $W/D$  and  $S/D$  must be sufficiently small to suppress the microstrip mode. The ratio  $(S + 2W)/2B$  must be small to suppress the rectangular coax mode.

This paper presents lumped element circuit models for several CCPW discontinuities, together with their element values as a function of frequency. The discontinuities characterized are an open circuit and a right angle bend. The measured frequency dependence of the effective dielectric constant,  $\epsilon(\text{eff})$ , and the unloaded quality factor,  $Q$ , are also presented for CCPW lines fabricated on  $\epsilon(r) = 2.2 \pm 0.02$  RT/Duroid 5880,  $\epsilon(r) = 6.0 \pm 0.15$  RT/Duroid 6006, and  $\epsilon(r) = 10.2 \pm 0.25$  3M Epsilam-10 substrates. This is followed by the design and characterization of a CCPW matched T-junction and a matched 1:3 junction. Lastly, the performance of a novel Coax-to-CCPW in-phase, N-way, radial power divider circuit is presented.

#### METHOD OF MEASUREMENTS

A resonator technique similar to that described by Richings (ref. 3) and Stephenson and Easter (ref. 4) was used. The  $\lambda/4$  end coupled stubs could not be etched off as in the case of microstrip since this would alter the CCPW open end parameters. Hence, a four resonator set had to be fabricated for each frequency to determine the end effects.

This will contribute some errors to the results because the resonator lengths and gaps will not be identical for the two  $\lambda/2$  and  $\lambda$  resonators. In addition, S and W varied slightly for each resonator set since the resonators were not processed in parallel. The circuit dimensions were measured to  $\pm 0.0002$  in. The coupling gaps were varied to maintain a coupling coefficient,  $\beta$ , less than 1. For most of the resonator sets,  $\beta < 0.3$ . This is a sufficient condition to minimize the loading of the resonator for transmission lines with  $Q \geq 100$  as are reported in this paper. The Q was determined through a technique given in reference 5.

### EFFECTIVE DIELECTRIC CONSTANT

The  $\epsilon(\text{eff})$  was measured over the frequency range of 3 to 18 GHz for several unshielded CCPW lines and the results are shown in figure 2. The CCPW lines have been modeled using reference 6 and the  $\epsilon(\text{eff})$  is plotted for each CCPW line.  $\epsilon(\text{eff})$  of GCPW calculated from the closed form expression of Ghione

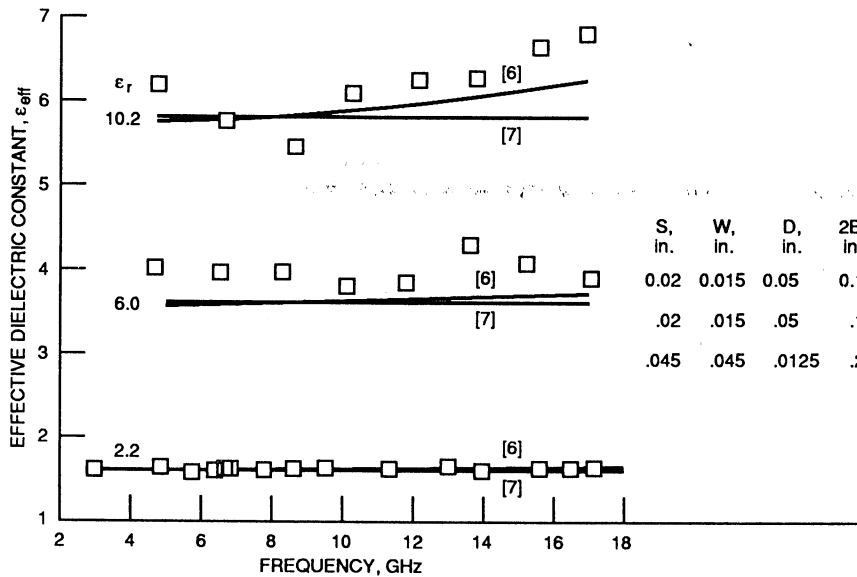


Figure 2. - Measured effective dielectric constant for unshielded CCPW as a function of frequency.

and Naldi (ref. 7) is also plotted for comparison. For the low dielectric substrate, either reference 6 or 7 could be used to predict  $\epsilon(\text{eff})$ . For the higher dielectric substrates, both methods predicted lower  $\epsilon(\text{eff})$  than what was measured.

### Effect of Substrate Thickness

$\epsilon(\text{eff})$  was measured as a function of frequency for unshielded CCPW lines fabricated on substrates with D in the range of 0.062 to 0.250 in. The CCPW parameters S, W, 2B, and  $\epsilon(r)$  were held fixed at 0.045 in., 0.010 in., 0.200 in., and 2.2, respectively. No variation in  $\epsilon(\text{eff})$  was observed for the thicker substrates,  $W/D \leq 1/12.5$ .  $\epsilon(\text{eff})$  of the thinner substrate,  $W/D \approx 1/6$ , was 0.7 percent higher than the other measured cases. This agrees with the calculated  $\epsilon(\text{eff})$  (ref. 6) and results in reference 2. The increase in  $\epsilon(\text{eff})$  is due to a microstrip mode.

To verify this, an RF probe was used to sample the electric fields under the center of the strip at the plane of the bottom conductor, the probe placement is shown in figure 3. Since odd mode CPW propagation has zero electric fields at this point, any fields measured by the probe must be due to a microstrip mode. The sampled field was measured for the thickest substrate and this value was used as a calibrated zero. No microstrip mode was measured as  $D$  was decreased until  $W/D \approx 1/6$ , when an increase in the sampled field amplitude of  $\approx 3$  dB was measured.

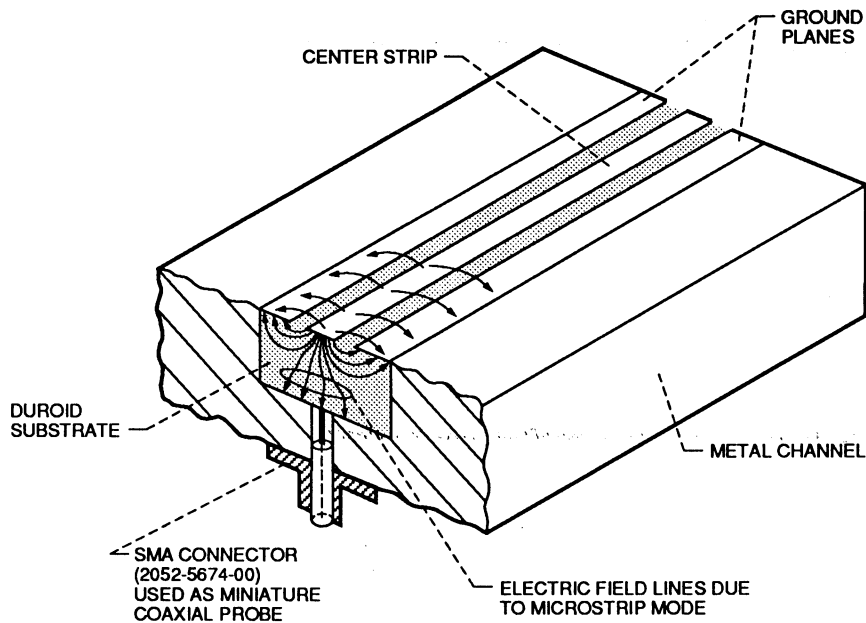


Figure 3. - Probe placement to sample the electric fields due to the microstrip mode.

### Effect of Cover Height

$\epsilon(\text{eff})$  was measured for shielded CCPW lines with cover heights of  $H = D$ ,  $2D$ , and  $4D$ . Resonators were tested with  $\epsilon(r)$ ,  $D$ ,  $S$ , and  $W$  equal to 2.2, 0.125 in., 0.045 in., and 0.010 in., respectively. Resonators were also fabricated on  $D = 0.050$  in.,  $\epsilon(r) = 6$  and 10.2 substrates. In all the cases, the change in  $\epsilon(\text{eff})$  from the unshielded case was negligible.

### LOSS MEASUREMENTS

#### Effect of $S$ and Shielding

Figure 4 shows the measured  $Q$  for resonators of length  $\lambda$  as a function of  $S$  for a fixed frequency. The  $Q$  of the unshielded resonators decreases with increasing  $S$  while the  $Q$  of the shielded resonators increases with increasing  $S$ . Therefore, radiation loss increases as  $S$  increases.

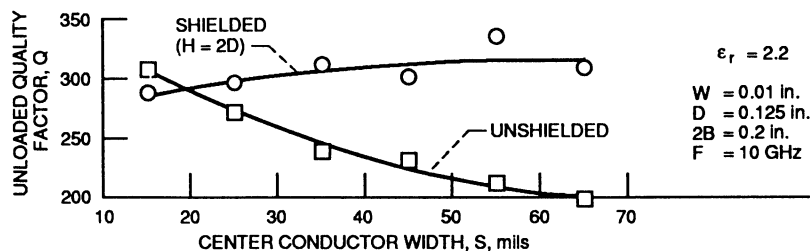


Figure 4. - Measured unloaded quality factor, Q, for CCPW as a function of the center conductor width, with and without a shielding enclosure.

### Effect of Frequency and Shielding

Figure 5 shows the measured Q over the frequency range of 3 to 18 GHz for  $\lambda$  resonators both with and without shielding. The reduction in Q with increasing frequency for the unshielded case is due to the increase in radiation loss. With shielding, the Q is observed to increase with frequency or the attenuation per unit wavelength decreases. A change in the cover height from  $H = 2D$  to  $H = D$  showed no measurable difference in Q.

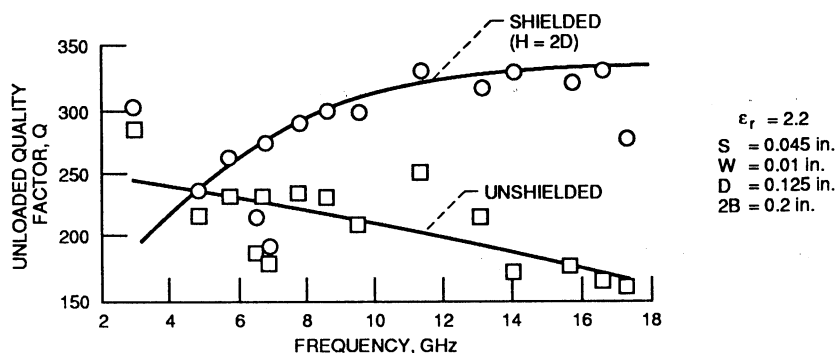


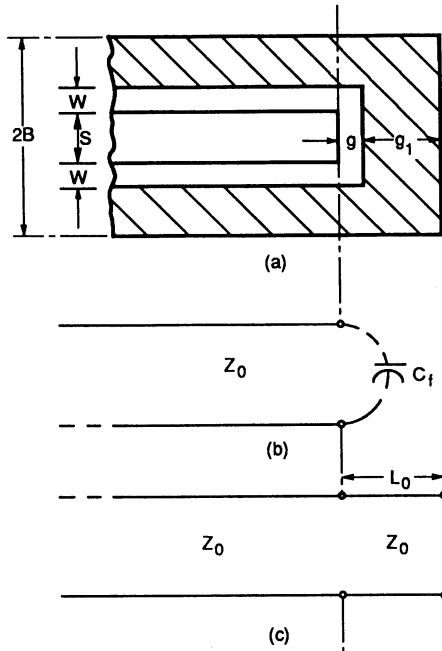
Figure 5. - Measured unloaded quality factor, Q, for CCPW as a function of frequency, with and without a shielding enclosure.

### Effect of D and $\epsilon(r)$

The effect of varying D in the range of 0.062 to 0.250 in. on Q was measured. No measurable variation in Q over the frequency range of 8 to 18 GHz was observed. CCPW resonators on the higher  $\epsilon(r)$  substrates had lower Q's. This is expected since the higher dielectric substrates concentrate more of the fields in the lossy substrate.

### CHANNELIZED CPW OPEN CIRCUIT

When a CPW line is terminated in an open circuit, there is an excess fringing of the electromagnetic fields which gives rise to a capacitance,  $C_f$  (ref. 8). This capacitance is equivalent to a short length of a transmission line,  $L_o$ , terminated in a perfect open circuit as illustrated in figure 6. The open end line extension for the unshielded CCPW de-embedded from the resonator data is shown as a function of frequency in figure 7. Although strict dimensional standards were used to select resonators, a large spread in  $L_o$  was present. The exact cause of this spread, particularly at the lower frequencies, is unexplained. There was no variation in  $L_o$  for resonators with a



(a) Schematic of a CCPW open circuit.  
 (b) Equivalent end fringing capacitance,  $C_f$ .  
 (c) Equivalent CCPW end-effect length,  $L_0$ .  
 Figure 6. - CCPW open circuit.

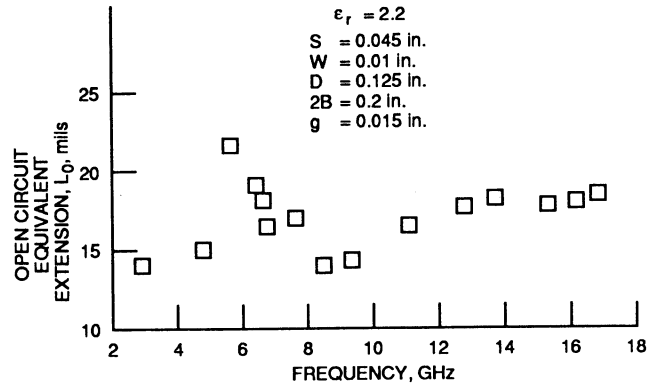


Figure 7. - Experimentally determined open circuit equivalent end-effect length as a function of frequency.

cover height of  $H \geq 2D$  since its presence has negligible effect on the fringing fields. Also,  $L_0$  was found to be independent of the distance between the open circuit and the end of the substrate,  $g_1$ .

### CHANNELIZED CPW RIGHT ANGLE BEND

A CCPW right angle bend and its equivalent circuit are shown in figure 8. The capacitance,  $C$ , is created by the accumulation of excess charge at the corners in the two slots and the resulting excess electric fields to the ground plane. The current flow interruption creates the excess inductance which can be equated to a length of transmission line,  $L$ . Radiation from the corner is represented by the shunt conductance,  $G_r$ .

To experimentally determine the capacitance,  $C$ , a voltage antinode has to be placed at the discontinuity. This is realized by placing a right angle bend at the center of an open circuit terminated resonator of length  $\lambda$ . To

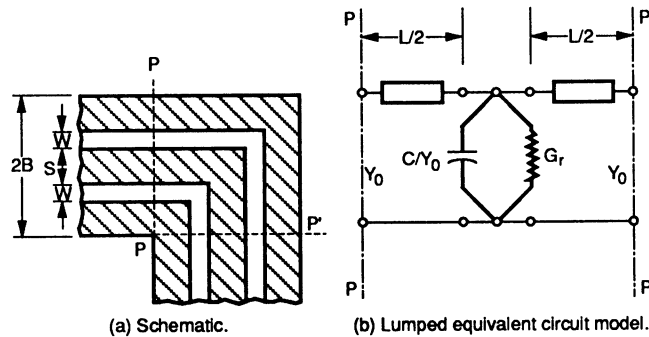


Figure 8. - CCPW right angle bend.

determine the inductance, a voltage node has to be placed at the discontinuity. This is realized by placing a right angle bend in the center of a  $\lambda/2$  resonator. The C and L are determined from the measured resonant frequencies using the following two equations (ref. 4):

$$L_n = \frac{nv}{2f_n \sqrt{\epsilon(\text{eff})}} - (l_n + L_o + L_g) \quad (1)$$

$$C/Y_o = \frac{1}{\pi f_2} \tan \left[ \frac{\pi f_2 \sqrt{\epsilon(\text{eff})} L_2}{v} \right] \quad (2)$$

where

$f_n \equiv$  resonant frequency of the  $n\lambda/2$  resonator

$L_g \equiv$  gap equivalent extension

$L_n \equiv$  Extension due to the parasitic reactance, either resulting from a voltage antinode for an  $n = 2$  resonator or a voltage node for an  $n = 1$  resonator

$L_o \equiv$  open circuit equivalent extension

$l_n \equiv$  physical length of the  $n\lambda/2$  resonator

$n \equiv$  order of resonance

$v \equiv 3 \times 10^8$  m/sec

The radiation conductance,  $G_r$ , was calculated by deriving a lumped element equivalent circuit model for the shielded and unshielded resonators incorporating a right angle bend (ref. 5). The difference in the resonator circuit conductance is then attributed to an equivalent radiation conductance. The model is valid near the resonant frequency. Table I presents the normalized capacitance  $C/Y_o$ , L, and the normalized radiation conductance  $G_r/Y_o$  as a function of the frequency. The radiation conductance is very small at low frequencies, however, it increases rapidly with frequency.

TABLE I. - CCPW RIGHT ANGLE  
BEND DISCONTINUITY

[S = 0.045 in., W = 0.010 in.,  $\epsilon(r) = 2.2$ ,  
2B = 0.200 in.]

Frequency, GHz	L, mil	C/Y <sub>o</sub> , pF·Ω	G <sub>r</sub> /Y <sub>o</sub>
2.97	22.622	4.219	0.0003635
4.92	26.241	4.353	.0014154
9.74	30.972	3.192	.010823
13.49	27.867	2.950	.011765
17.84	31.794	3.848	-----

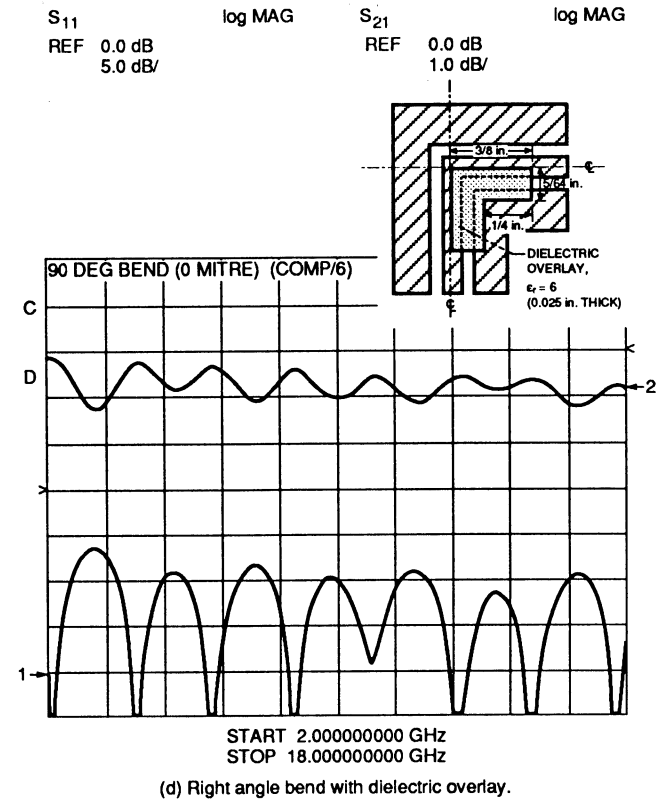
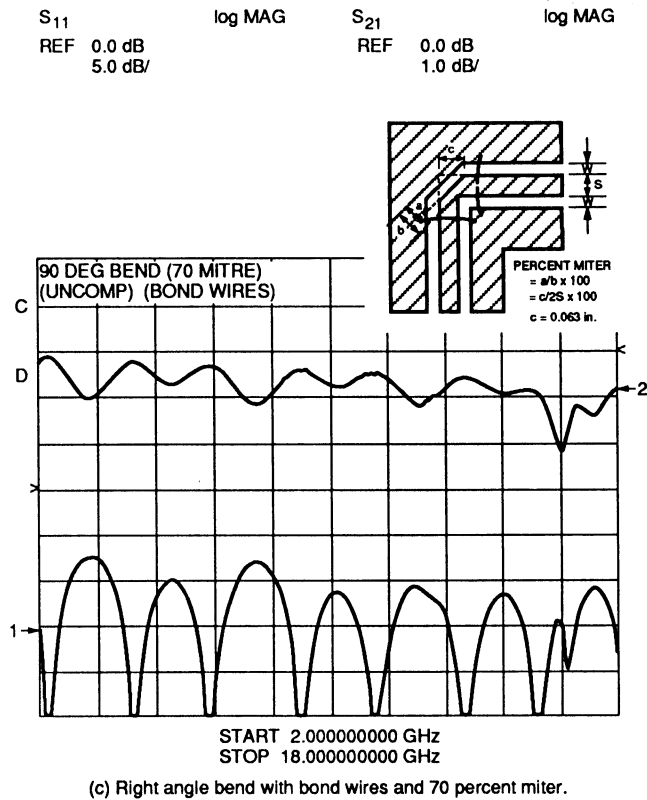
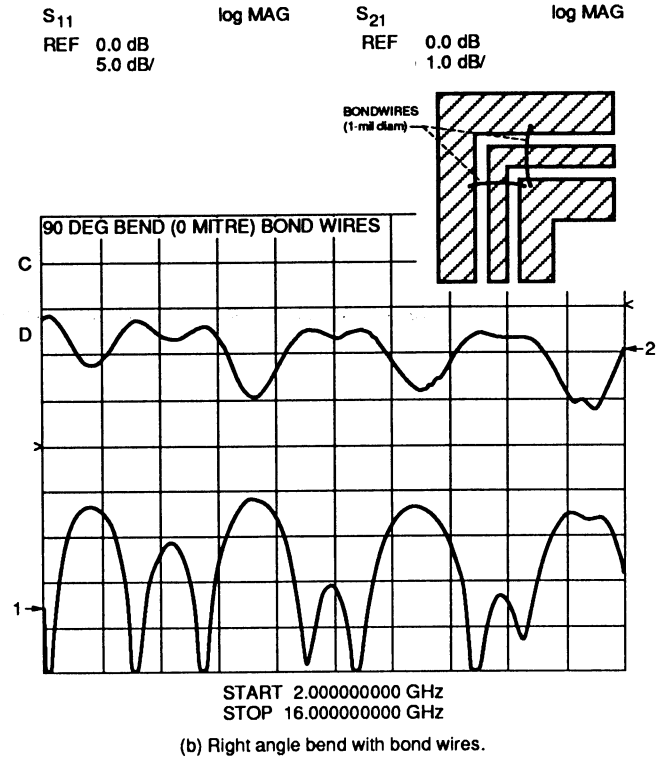
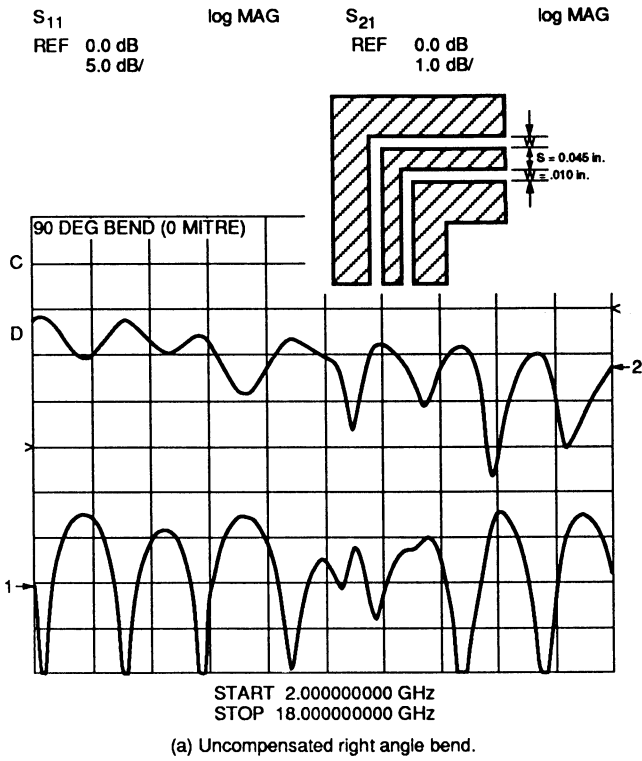


Figure 9. - Measured RF characteristics for CCPW right angle bends with configurations inset.

The path length differences between the two slots at the CCPW right angle bend degrade the RF characteristics. Therefore, compensating techniques such as miters (ref. 9) and dielectric overlays (ref. 8) were investigated. Figure 9 illustrates a CCPW right angle bend and three possible compensating techniques and shows the measured insertion and return loss for each of the bends. The use of bond wires (fig. 9(b)), to hold the ground planes to the same potential at the element reference planes reduced the resonances in the insertion loss characteristics. To further reduce the path length difference, miters as large as 70 percent were tried. The miter and bond wires eliminated most of the resonances (fig. 9(c)). Finally, a dielectric overlay was placed on the inner slot (fig. 9(d)). The overlay slows the signal travelling along the inner slot so the signal emerging from each of the slots after the right angle bend is in phase. As shown in figure 9(d), the insertion loss and the return loss were less than 1.0 dB and greater than 10 dB, respectively, over a 2 to 18 GHz band. This agrees with the characteristics of a straight thru circuit.

### CHANNELIZED CPW MATCHED T-JUNCTION

A pen-plot of a CCPW matched T-junction is shown in figure 10. At the T-junction, the characteristic impedance of the two side arms,  $Z_1$ , are in parallel and the net impedance the input arm sees is  $Z_1/2$ . Therefore, for impedance matching, the characteristic impedance,  $Z_0$ , of the feed arm was set equal to  $Z_1/2$ . To accomplish this, the output arms were tapered to an impedance of  $\approx 135 \Omega$  and the input arm was tapered to  $\approx 67 \Omega$ . At the coax-to-CCPW transitions, the CCPW impedance was  $\approx 70 \Omega$  to provide a good match to the  $50 \Omega$  coaxial line (ref. 8). When a shielding cover of height  $H = D$  was used, an insertion loss and return loss of 0.5 dB and 10 dB, respectively, were measured up to 12.5 GHz. A pair of bond wires were added to hold the ground planes at the junction at the same potential (refs. 10 and 11). This increased the bandwidth to 16.5 GHz. The measured insertion loss and return loss of the T-junction with bond wires are presented in figure 11. When the bond wires were used, the measured insertion loss and return loss was independent of the use of a cover.

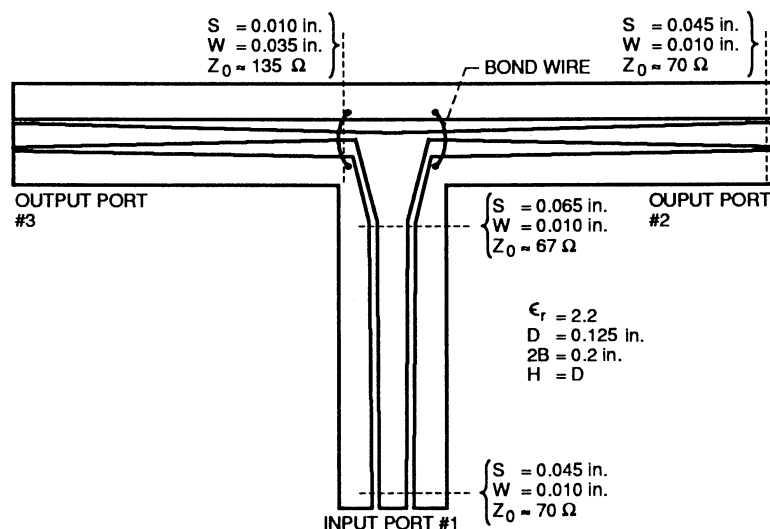


Figure 10. - Pen-plot of a CCPW matched T-junction.

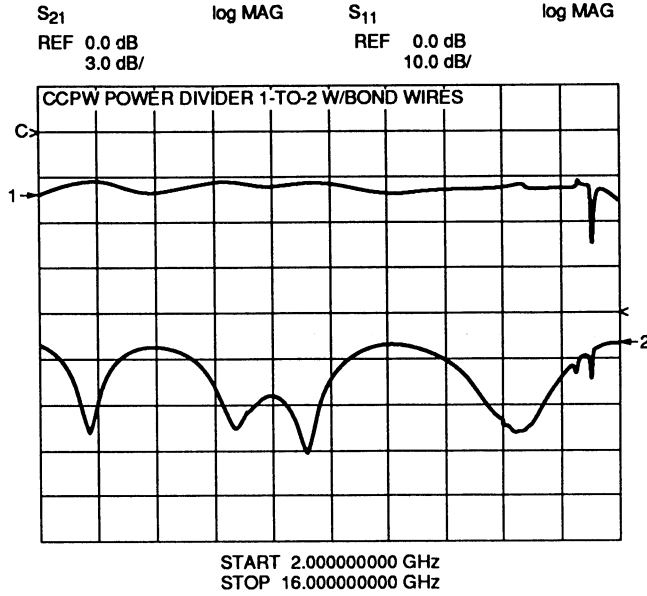


Figure 11. - Measured amplitude of the power coupled to one of the output ports and the return loss of the input port for a CCPW matched T-junction.

### CHANNELIZED CPW MATCHED 1:3 JUNCTION

A pen-plot of a CCPW matched 1:3 junction is shown in figure 12. The output arms have been tapered to  $\approx 135 \Omega$  at the junction. The input arm was tapered to  $45 \Omega$  for impedance matching. When a shielding enclosure of height  $H = D$  was used, a return loss greater than 10 dB and low insertion loss was measured through 12.5 GHz. However, a maximum phase imbalance between ports 2 and 3 of  $\approx 70^\circ$  exists at 12.5 GHz.

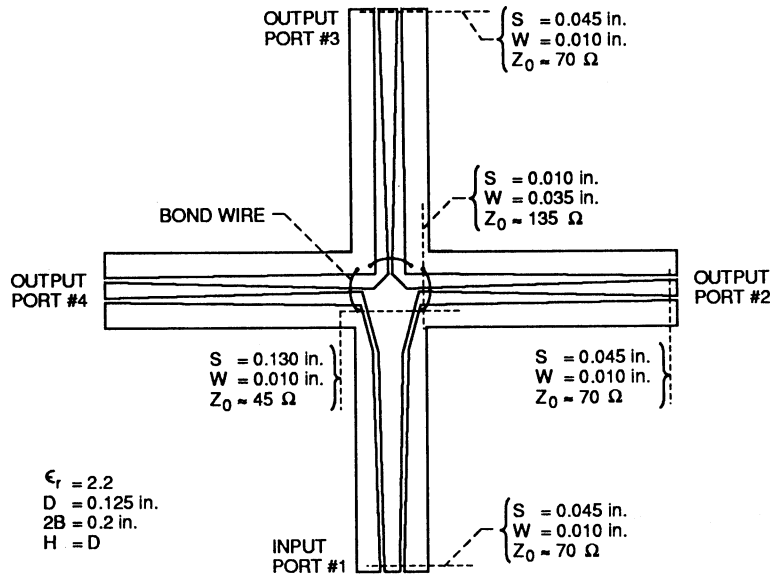


Figure 12. - Pen-plot of CCPW matched 1-to-3 junction.

The use of three bond wires as shown in figure 12 increased the bandwidth to 16.0 GHz. In addition, the bond wires reduced the phase imbalance between ports 2 and 3 by  $20^\circ$  at 12.5 GHz. The measured insertion loss and return loss of the three-way junction with bond wires are presented in figure 13. The average measured amplitude of  $-5$  dB at the output ports agrees well with the expected  $-4.8$  dB. There was negligible amplitude and phase imbalance between ports 2 and 4. A maximum of 1 dB of amplitude imbalance was measured between ports 2 and 3. The phase imbalance between ports 2 and 3 increased linearly from  $\approx 0^\circ$  at 2 GHz to  $70^\circ$  at 16 GHz. The use of a shielding enclosure with the bond wires did not result in any further improvement in the characteristics.

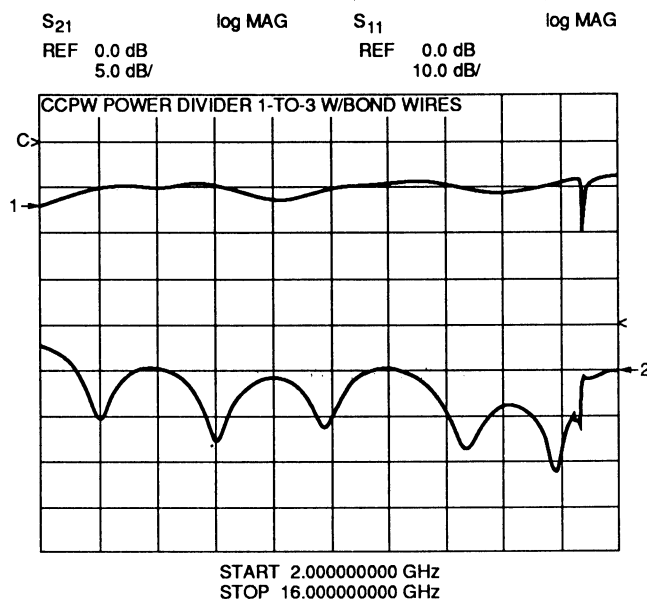


Figure 13. - Measured amplitude of the power coupled to one of the output ports and the return loss of the coaxial input port for a CCPW matched 1-to-3 junction.

#### COAX-to-CHANNELIZED CPW IN-PHASE N-WAY RADIAL POWER DIVIDER

A coax-to-CCPW in-phase, four-way radial power divider is shown in figure 14. The junction is formed by the intersection of four CCPW lines. Power is coupled to this junction from a coaxial cable whose outer conductor is slotted along the  $z$  direction to form four coupled transmission lines. The center pin of the coaxial line meets the intersecting CCPW center conductors while the four coupled outer conductors meet the CCPW ground planes. Therefore, the electric current at the open end of the coax is divided into the four CCPW lines as illustrated in figure 15. This arrangement has the advantage of holding the ground planes at the same potential and exciting the four CCPW lines in equal amplitude and phase without the need for bond wires. Each of the four CCPW lines, figure 16, has an impedance of  $135 \Omega$  at the junction. Therefore, the net impedance seen by the coaxial line is  $\approx 34 \Omega$ . A quarter wave coaxial dielectric transformer ( $\epsilon(r) = 4$ ) was used at the junction to match the  $50 \Omega$  coaxial line to the  $34 \Omega$  CCPW junction impedance. Each of the three pairs of slits in the ground plane of the CCPW acts as a stub and helps improve the CCPW to coaxial connector impedance match over the measured frequency range.

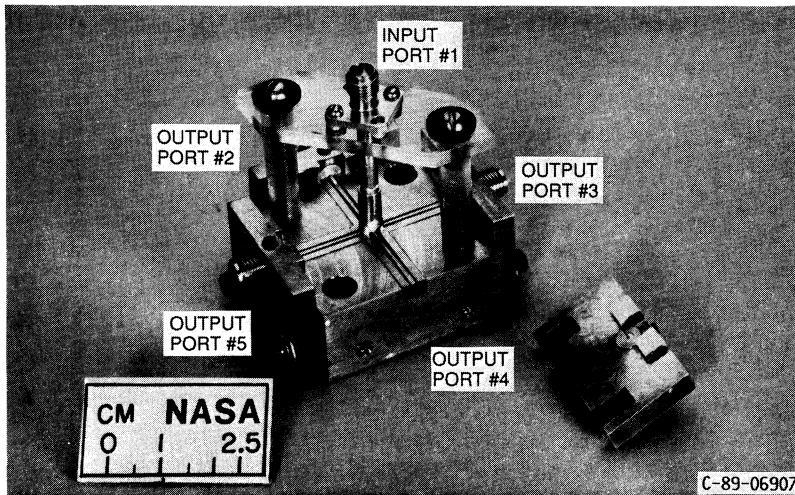


Figure 14. - Coax-to-CCPW in-phase, four-way, radial power divider.

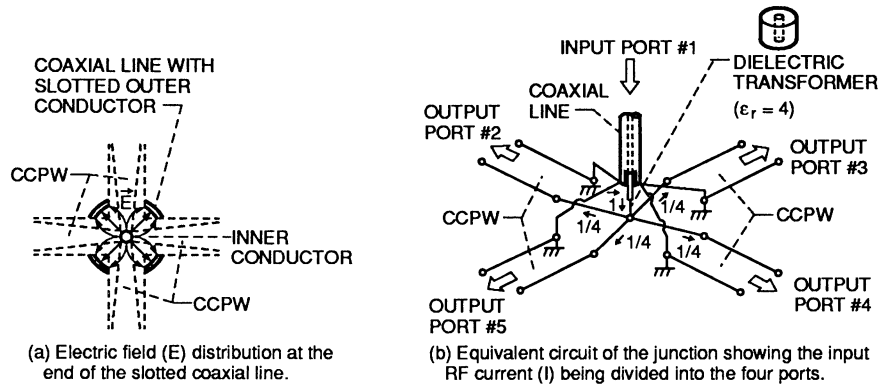


Figure 15. - Coax-to-CCPW junction.

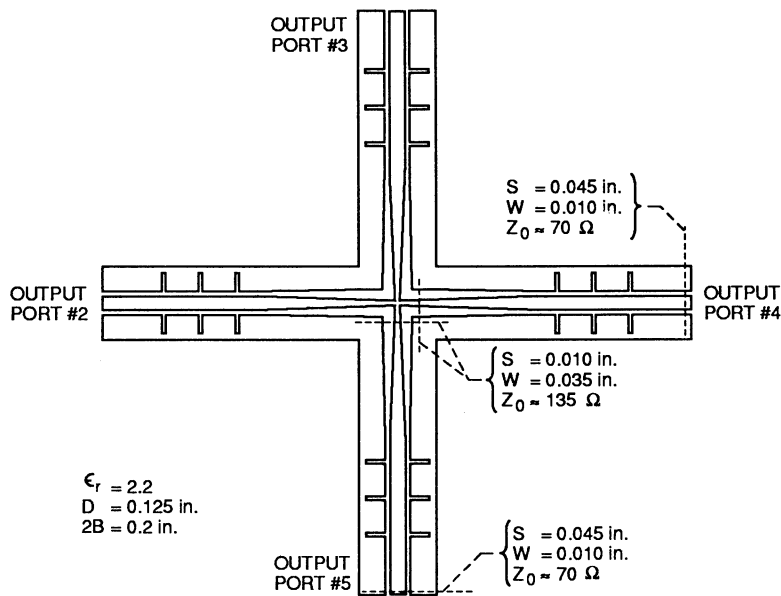


Figure 16. - Pen-plot of the coax-to-CCPW in-phase, four-way, radial power divider.

The measured amplitude of the power coupled to one of the output ports over an octave bandwidth is shown in figure 17 and is typical of the junction. The  $-6.5$  dB measured amplitude at the output ports is in good agreement with the  $-6.0$  dB expected for a 1:4 junction. The additional loss includes the CCPW to coaxial transformer and connector losses. Also superimposed on figure 18 is the return loss of the input port. Figure 18 is a measurement of the amplitude and phase balance for the four output ports; the amplitude and phase balance are within  $0.5$  dB and  $5^\circ$ , respectively. These values are a function of the mechanical structure itself since all of the ports are identical. The isolation between the ports is  $\approx 10$  dB.

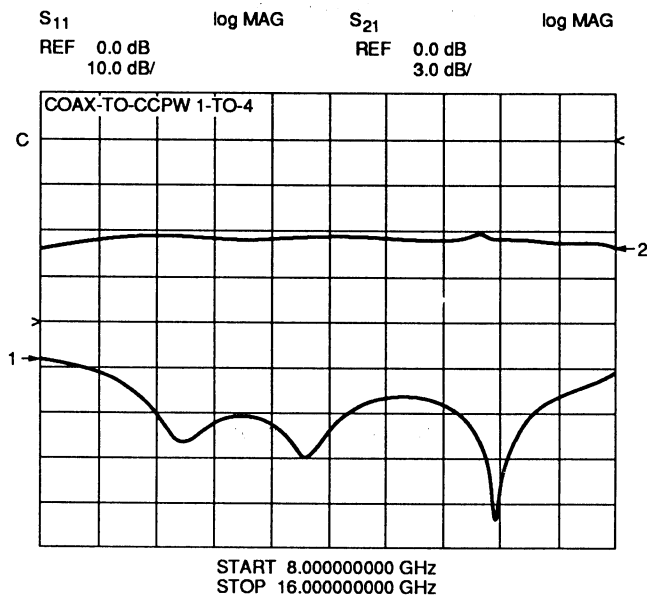


Figure 17. - Measured amplitude of the power coupled to one of the output ports and the return loss of the coaxial input port for a four-way radial power divider.

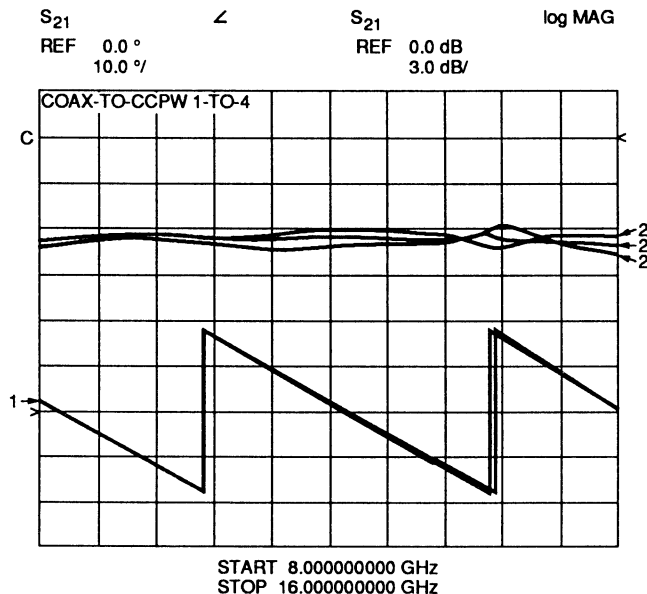


Figure 18. - Measured amplitude and phase balance for a coax-to-CCPW four-way power divider.

A coax-to-CCPW two-way radial power divider with the same basic structure as that described above was fabricated. The outer conductor of the coaxial line was slotted to form two coupled transmission lines. A dielectric transformer was not used with this structure. The measured amplitude at the output ports and the return loss at the coax input port are presented in figure 19. The amplitude imbalance for this circuit is less than 0.5 dB and the phase imbalance is less than 5°. Again, these values are dependent on the mechanical realization of the power divider.

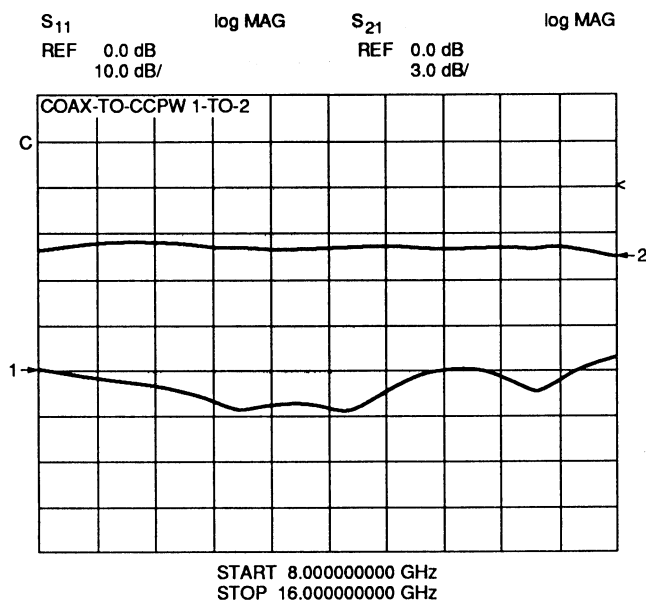


Figure 19. - Measured amplitude of the power coupled to one of the output ports and the return loss of the coaxial input port for a two-way radial power divider.

## CONCLUSIONS

A new variant of CPW which has been termed CCPW has been demonstrated. The propagation characteristics of this structure show it to be useful for wide bandwidth, low loss microwave circuits where the favorable size advantage of CCPW over rectangular waveguide may be needed. Equivalent circuit model element values are presented for a CCPW open circuit and a CCPW right angle bend. A matched CCPW T-junction, a matched 1:3 junction, and a novel coax-to-CCPW in-phase, N-way, radial power divider are also demonstrated. These exhibit low loss and wide bandwidth and hence should facilitate the implementation of CCPW in microwave signal distribution networks such as in a phased array antenna system.

## REFERENCES

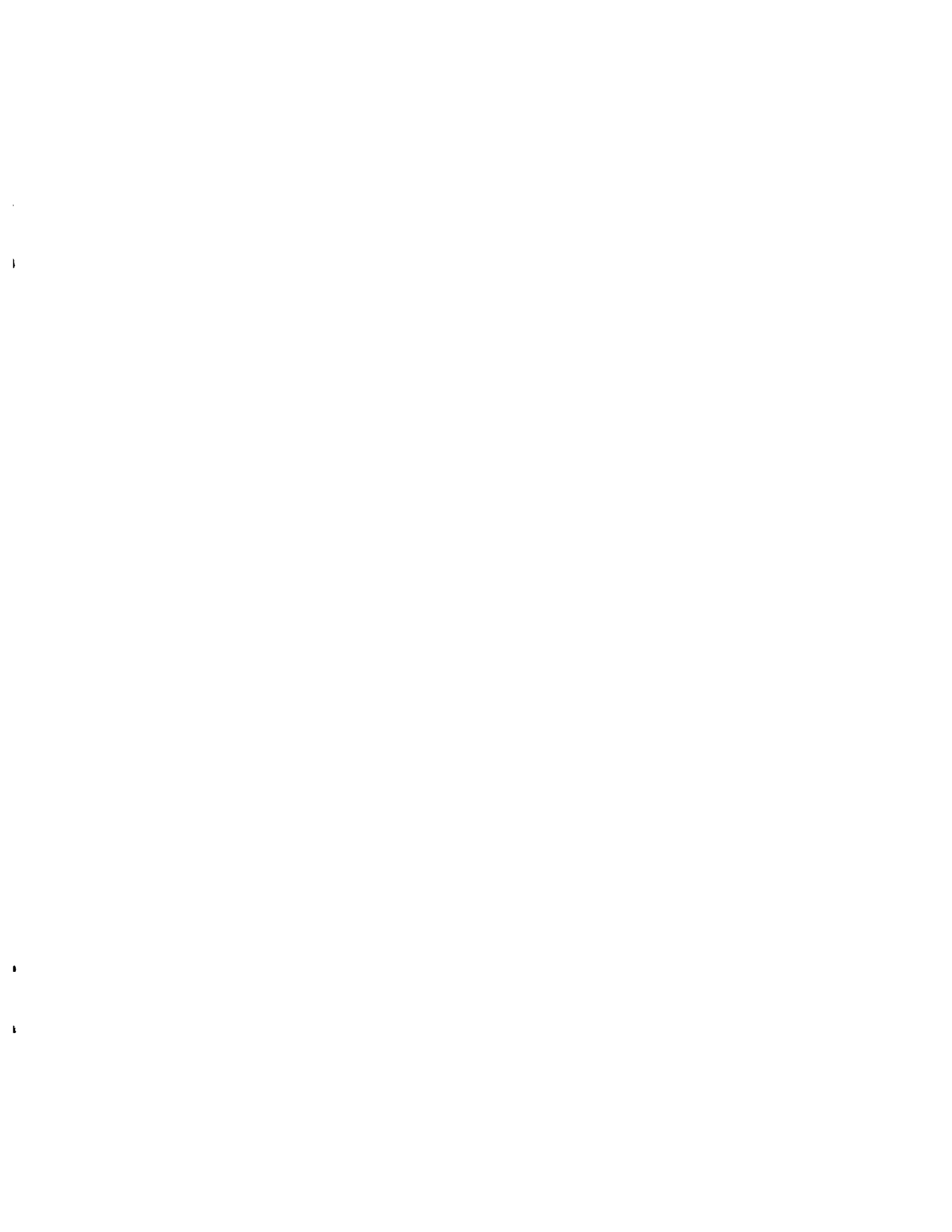
1. Wen, C.P.: Coplanar Waveguide: A Surface Strip Transmission Line Suitable for Nonreciprocal Gyromagnetic Device Applications. IEEE Trans. Microwave Theory Tech., vol. MTT-17, no. 12, Dec. 1969, pp. 1087-1090.
2. Shih, Y.C.; and Itoh, T.: Analysis of Conductor-Backed Coplanar Waveguide. Electron. Lett., vol. 18, no. 12, June 10, 1982, pp. 538-540.

3. Richings, J.G.: An Accurate Experimental Method for Determining the Important Properties of Microstrip Transmission Lines. *Marconi Rev.*, vol. 37, no. 195, 1974, pp. 209-216.
4. Stephenson, I.M.; and Easter, B.: Resonant Techniques for Establishing the Equivalent Circuits of Small Discontinuities in Microstrip. *Electron. Lett.*, vol. 7, no. 19, Sept. 23, 1971, pp. 582-584.
5. Romanofsky, R.R.: Analytical and Experimental Procedures for Determining Propagation Characteristics of mm-Wave GaAs Microstrip Lines. NASA TP-2899, 1989.
6. Simons, R.N.: Suspended Coupled Slotline Using Double Layer Dielectric. *IEEE Trans. Microwave Theory Tech.*, vol. MTT-29, no. 2, Feb. 1981, pp. 162-165.
7. Ghione, G.; and Naldi, C.: Parameters of Coplanar Waveguides with Lower Ground Plane. *Electron. Lett.*, vol. 19, no. 18, Sept. 1, 1983, pp. 734-735.
8. Simons, R.N.; and Ponchak, G.E.: Modeling of Some Coplanar Waveguide Discontinuities. *IEEE Trans. Microwave Theory Tech.*, vol. MTT 36, no. 12, Dec. 1988, pp. 1796-1803.
9. Douville, R.J.P.; and James, D.S.: Experimental Study of Symmetric Microstrip Bends and Their Compensation. *IEEE Trans. Microwave Theory Tech.*, vol. MTT-26, no. 3, Mar. 1978, pp. 175-182.
10. Houdart, M.: Coplanar Lines: Application to Broadband Microwave Integrated Circuits. 6th European Microwave Conference, Microwave Exhibitions and Publishers Ltd., Sevenoaks, England, 1976, pp. 49-53.
11. Stegens, R.E.: Coplanar Waveguide FET Amplifiers for Satellite Communications Systems. *Comsat Tech. Rev.*, vol. 9, no. 1, Spring 1979, pp. 255-267.



## Report Documentation Page

<b>1. Report No.</b> NASA TM-102494	<b>2. Government Accession No.</b>	<b>3. Recipient's Catalog No.</b>	
<b>4. Title and Subtitle</b> Experimental Investigations on Channelized Coplanar Waveguide		<b>5. Report Date</b> April 1990	
		<b>6. Performing Organization Code</b>	
<b>7. Author(s)</b> Rainee N. Simons, George E. Ponchak, Konstantinos S. Martzaklis, and Robert R. Romanofsky		<b>8. Performing Organization Report No.</b> E-5285	
		<b>10. Work Unit No.</b> 506-44-2C	
<b>9. Performing Organization Name and Address</b> National Aeronautics and Space Administration Lewis Research Center Cleveland, Ohio 44135-3191		<b>11. Contract or Grant No.</b>	
		<b>13. Type of Report and Period Covered</b> Technical Memorandum	
<b>12. Sponsoring Agency Name and Address</b> National Aeronautics and Space Administration Washington, D.C. 20546-0001		<b>14. Sponsoring Agency Code</b>	
		<b>15. Supplementary Notes</b> Rainee N. Simons, Case Western Reserve University, Cleveland, Ohio 44106 and NASA Resident Research Associate at Lewis Research Center (work funded by NASA Grant NAG3-816). George E. Ponchak and Robert R. Romanofsky, NASA Lewis Research Center. Konstantinos S. Martzaklis, University of Akron, Akron, Ohio 44325 and Student Co-Op at Lewis Research Center.	
<b>16. Abstract</b> <p>This paper presents a new variant of coplanar waveguide (CPW) which has been termed channelized coplanar waveguide (CCPW). Measured propagation characteristics for CCPW such as <math>\epsilon(\text{eff})</math> and unloaded Q as a function of geometrical parameters and frequency are presented. The measured and modelled <math>\epsilon(\text{eff})</math> are also compared. Equivalent circuit model element values are presented for a CCPW open circuit and a CCPW right angle bend. A CCPW matched T-junction, matched 1:3 junction, and a novel coax-to-CCPW in-phase, N-way, radial power divider are also demonstrated.</p>			
<b>17. Key Words (Suggested by Author(s))</b> Waveguide Coplanar waveguide Power dividers		<b>18. Distribution Statement</b> Unclassified - Unlimited Subject Category 33	
<b>19. Security Classif. (of this report)</b> Unclassified	<b>20. Security Classif. (of this page)</b> Unclassified	<b>21. No. of pages</b> 16	<b>22. Price*</b> A03



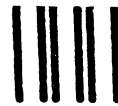
National Aeronautics and  
Space Administration

**Lewis Research Center**  
Cleveland, Ohio 44135

**Official Business**  
**Penalty for Private Use \$300**

**FOURTH CLASS MAIL**

**ADDRESS CORRECTION REQUESTED**



Postage and Fees Paid  
National Aeronautics and  
Space Administration  
NASA-451

**NASA**

---